Research Article | Vol. 25, No. 18 | 4 Sep 2017 | OPTICS EXPRESS 21115
Optics EXPRESS

Broadband two-dimensional electronic spectroscopy in an actively phase stabilized pump-probe configuration

WEIDA ZHU,[1] RUI WANG,[1] CHUNFENG ZHANG,[1,*] GUODONG WANG,[1] YUNLONG LIU,[1] WEI ZHAO,[2] XINGCAN DAI,[2] XIAOYONG WANG,[1] GIULIO CERULLO,[3] STEVEN CUNDIFF,[4] AND MIN XIAO[1,5]

[1]*National Laboratory of Solid State Microstructures, School of Physics, and Collaborative Innovation Center of Advanced Microstructures, Nanjing University, Nanjing 210093, China*

[2]*Department of Physics, Tsinghua University, Beijing 100084, China*

[3]*IFN-CNR, Dipartimento di Fisica, Politecnico di Milano, Piazza Leonardo da Vinci 32, 20133 Milano, Italy*

[4]*Department of Physics, University of Michigan, Ann Arbor, Michigan 48109, USA*

[5]*Department of Physics, University of Arkansas, Fayetteville, Arkansas 72701, USA*

**cfzhang@nju.edu.cn*

Abstract: We introduce a novel configuration for two-dimensional electronic spectroscopy (2DES) that combines the partially collinear pump-probe geometry with active phase locking. We demonstrate the method on a solution sample of CdSe/ZnS nanocrystals by employing two non-collinear optical parametric amplifiers as the pump and probe sources. The two collinear pump pulse replicas are created using a Mach-Zehnder interferometer phase stabilized by active feedback electronics. Taking the advantage of separated paths of the two pump pulses in the interferometer, we improve the signal-to-noise ratio with double modulation of the individual pump beams. In addition, a quartz wedge pair manipulates the phase difference between the two pump pulses, enabling the recovery of the rephasing and non-rephasing signals. Our setup integrates many advantages of available 2DES techniques with robust phase stabilization, ultrafast time resolution, two-color operation, long delay scan, individual polarization manipulation and the ease of implementation.

OCIS codes: (300.6300) Spectroscopy, Fourier transforms; (300.6530) Spectroscopy, ultrafast; (120.3180) Interferometry.

References and links

1. N. S. Ginsberg, Y.-C. Cheng, and G. R. Fleming, "Two-dimensional electronic spectroscopy of molecular aggregates," Acc. Chem. Res. **42**(9), 1352–1363 (2009).
2. M. Cho, "Coherent two-dimensional optical spectroscopy," Chem. Rev. **108**(4), 1331–1418 (2008).
3. D. M. Jonas, "Two-dimensional femtosecond spectroscopy," Annu. Rev. Phys. Chem. **54**(1), 425–463 (2003).
4. S. T. Cundiff and S. Mukamel, "Optical multidimensional coherent spectroscopy," Phys. Today **66**(7), 44–49 (2013).
5. P. Hamm and M. T. Zanni, *Concepts and Methods of 2D Infrared Spectroscopy* (Cambridge University Pres, 2011).
6. G. Moody, C. Kavir Dass, K. Hao, C.-H. Chen, L.-J. Li, A. Singh, K. Tran, G. Clark, X. Xu, G. Berghäuser, E. Malic, A. Knorr, and X. Li, "Intrinsic homogeneous linewidth and broadening mechanisms of excitons in monolayer transition metal dichalcogenides," Nat. Commun. **6**, 8315 (2015).
7. A. E. Almand-Hunter, H. Li, S. T. Cundiff, M. Mootz, M. Kira, and S. W. Koch, "Quantum droplets of electrons and holes," Nature **506**(7489), 471–475 (2014).
8. D. B. Turner and K. A. Nelson, "Coherent measurements of high-order electronic correlations in quantum wells," Nature **466**(7310), 1089–1092 (2010).
9. K. W. Stone, K. Gundogdu, D. B. Turner, X. Li, S. T. Cundiff, and K. A. Nelson, "Two-quantum 2D FT electronic spectroscopy of biexcitons in GaAs quantum wells," Science **324**(5931), 1169–1173 (2009).
10. F. D. Fuller, J. Pan, A. Gelzinis, V. Butkus, S. S. Senlik, D. E. Wilcox, C. F. Yocum, L. Valkunas, D. Abramavicius, and J. P. Ogilvie, "Vibronic coherence in oxygenic photosynthesis," Nat. Chem. **6**(8), 706–711 (2014).

#301609 https://doi.org/10.1364/OE.25.021115
Journal © 2017 Received 3 Jul 2017; revised 12 Aug 2017; accepted 15 Aug 2017; published 21 Aug 2017

Optics EXPRESS

11. J. Lim, D. Paleček, F. Caycedo-Soler, C. N. Lincoln, J. Prior, H. von Berlepsch, S. F. Huelga, M. B. Plenio, D. Zigmantas, and J. Hauer, "Vibronic origin of long-lived coherence in an artificial molecular light harvester," Nat. Commun. **6**, 7755 (2015).
12. T. Brixner, J. Stenger, H. M. Vaswani, M. Cho, R. E. Blankenship, and G. R. Fleming, "Two-dimensional spectroscopy of electronic couplings in photosynthesis," Nature **434**(7033), 625–628 (2005).
13. E. Collini, C. Y. Wong, K. E. Wilk, P. M. G. Curmi, P. Brumer, and G. D. Scholes, "Coherently wired light-harvesting in photosynthetic marine algae at ambient temperature," Nature **463**(7281), 644–647 (2010).
14. D. Hayes, G. B. Griffin, and G. S. Engel, "Engineering coherence among excited states in synthetic heterodimer systems," Science **340**(6139), 1431–1434 (2013).
15. H. Lee, Y.-C. Cheng, and G. R. Fleming, "Coherence dynamics in photosynthesis: Protein protection of excitonic coherence," Science **316**(5830), 1462–1465 (2007).
16. V. Tiwari, W. K. Peters, and D. M. Jonas, "Electronic resonance with anticorrelated pigment vibrations drives photosynthetic energy transfer outside the adiabatic framework," Proc. Natl. Acad. Sci. U.S.A. **110**(4), 1203–1208 (2013).
17. G. S. Engel, T. R. Calhoun, E. L. Read, T.-K. Ahn, T. Mancal, Y.-C. Cheng, R. E. Blankenship, and G. R. Fleming, "Evidence for wavelike energy transfer through quantum coherence in photosynthetic systems," Nature **446**(7137), 782–786 (2007).
18. A. De Sio, F. Troiani, M. Maiuri, J. Réhault, E. Sommer, J. Lim, S. F. Huelga, M. B. Plenio, C. A. Rozzi, G. Cerullo, E. Molinari, and C. Lienau, "Tracking the coherent generation of polaron pairs in conjugated polymers," Nat. Commun. **7**, 13742 (2016).
19. Y. Song, S. N. Clafton, R. D. Pensack, T. W. Kee, and G. D. Scholes, "Vibrational coherence probes the mechanism of ultrafast electron transfer in polymer-fullerene blends," Nat. Commun. **5**, 4933 (2014).
20. S. M. Falke, C. A. Rozzi, D. Brida, M. Maiuri, M. Amato, E. Sommer, A. De Sio, A. Rubio, G. Cerullo, E. Molinari, and C. Lienau, "Coherent ultrafast charge transfer in an organic photovoltaic blend," Science **344**(6187), 1001–1005 (2014).
21. G. D. Scholes, G. R. Fleming, L. X. Chen, A. Aspuru-Guzik, A. Buchleitner, D. F. Coker, G. S. Engel, R. van Grondelle, A. Ishizaki, D. M. Jonas, J. S. Lundeen, J. K. McCusker, S. Mukamel, J. P. Ogilvie, A. Olaya-Castro, M. A. Ratner, F. C. Spano, K. B. Whaley, and X. Zhu, "Using coherence to enhance function in chemical and biophysical systems," Nature **543**(7647), 647–656 (2017).
22. G. D. Scholes, G. R. Fleming, A. Olaya-Castro, and R. van Grondelle, "Lessons from nature about solar light harvesting," Nat. Chem. **3**(10), 763–774 (2011).
23. J.-L. Brédas, E. H. Sargent, and G. D. Scholes, "Photovoltaic concepts inspired by coherence effects in photosynthetic systems," Nat. Mater. **16**(1), 35–44 (2016).
24. J. D. Hybl, A. W. Albrecht, S. M. G. Faeder, and D. M. Jonas, "Two-dimensional electronic spectroscopy," Chem. Phys. Lett. **297**(3-4), 307–313 (1998).
25. T. Brixner, I. V. Stiopkin, and G. R. Fleming, "Tunable two-dimensional femtosecond spectroscopy," Opt. Lett. **29**(8), 884–886 (2004).
26. M. L. Cowan, J. P. Ogilvie, and R. J. D. Miller, "Two-dimensional spectroscopy using diffractive optics based phased-locked photon echoes," Chem. Phys. Lett. **386**(1-3), 184–189 (2004).
27. J. A. Myers, K. L. M. Lewis, P. F. Tekavec, and J. P. Ogilvie, "Two-color two-dimensional Fourier transform electronic spectroscopy with a pulse-shaper," Opt. Express **16**(22), 17420–17428 (2008).
28. S.-H. Shim and M. T. Zanni, "How to turn your pump-probe instrument into a multidimensional spectrometer: 2D IR and Vis spectroscopies via pulse shaping," Phys. Chem. Chem. Phys. **11**(5), 748–761 (2009).
29. J. Réhault, M. Maiuri, A. Oriana, and G. Cerullo, "Two-dimensional electronic spectroscopy with birefringent wedges," Rev. Sci. Instrum. **85**(12), 123107 (2014).
30. R. Borrego-Varillas, A. Oriana, L. Ganzer, A. Trifonov, I. Buchvarov, C. Manzoni, and G. Cerullo, "Two-dimensional electronic spectroscopy in the ultraviolet by a birefringent delay line," Opt. Express **24**(25), 28491–28499 (2016).
31. L. P. Deflores, R. A. Nicodemus, and A. Tokmakoff, "Two-dimensional Fourier transform spectroscopy in the pump-probe geometry," Opt. Lett. **32**(20), 2966–2968 (2007).
32. J. Helbing and P. Hamm, "Compact implementation of Fourier transform two-dimensional IR spectroscopy without phase ambiguity," J. Opt. Soc. Am. B **28**(1), 171–178 (2011).
33. A. D. Bristow, D. Karaiskaj, X. Dai, T. Zhang, C. Carlsson, K. R. Hagen, R. Jimenez, and S. T. Cundiff, "A versatile ultrastable platform for optical multidimensional Fourier-transform spectroscopy," Rev. Sci. Instrum. **80**(7), 073108 (2009).
34. N. Belabas and M. Joffre, "Visible-infrared two-dimensional Fourier-transform spectroscopy," Opt. Lett. **27**(22), 2043–2045 (2002).
35. V. Volkov, R. Schanz, and P. Hamm, "Active phase stabilization in Fourier-transform two-dimensional infrared spectroscopy," Opt. Lett. **30**(15), 2010–2012 (2005).
36. A. Al Haddad, A. Chauvet, J. Ojeda, C. Arrell, F. van Mourik, G. Auböck, and M. Chergui, "Set-up for broadband Fourier-transform multidimensional electronic spectroscopy," Opt. Lett. **40**(3), 312–315 (2015).
37. B. Spokoyny, C. J. Koh, and E. Harel, "Stable and high-power few cycle supercontinuum for 2D ultrabroadband electronic spectroscopy," Opt. Lett. **40**(6), 1014–1017 (2015).
38. X. Ma, J. Dostál, and T. Brixner, "Broadband 7-fs diffractive-optic-based 2D electronic spectroscopy using hollow-core fiber compression," Opt. Express **24**(18), 20781–20791 (2016).

Optics EXPRESS

39. N. M. Kearns, R. D. Mehlenbacher, A. C. Jones, and M. T. Zanni, "Broadband 2D electronic spectrometer using white light and pulse shaping: noise and signal evaluation at 1 and 100 kHz," Opt. Express **25**(7), 7869–7883 (2017).
40. A. Ghosh, A. L. Serrano, T. A. Oudenhoven, J. S. Ostrander, E. C. Eklund, A. F. Blair, and M. T. Zanni, "Experimental implementations of 2D IR spectroscopy through a horizontal pulse shaper design and a focal plane array detector," Opt. Lett. **41**(3), 524–527 (2016).
41. P. F. Tekavec, G. A. Lott, and A. H. Marcus, "Fluorescence-detected two-dimensional electronic coherence spectroscopy by acousto-optic phase modulation," J. Chem. Phys. **127**(21), 214307 (2007).
42. G. Nardin, T. M. Autry, K. L. Silverman, and S. T. Cundiff, "Multidimensional coherent photocurrent spectroscopy of a semiconductor nanostructure," Opt. Express **21**(23), 28617–28627 (2013).
43. K. J. Karki, J. R. Widom, J. Seibt, I. Moody, M. C. Lonergan, T. Pullerits, and A. H. Marcus, "Coherent two-dimensional photocurrent spectroscopy in a PbS quantum dot photocell," Nat. Commun. **5**, 5869 (2014).
44. A. A. Bakulin, C. Silva, and E. Vella, "Ultrafast Spectroscopy with Photocurrent Detection: Watching Excitonic Optoelectronic Systems at Work," J. Phys. Chem. Lett. **7**(2), 250–258 (2016).
45. S. Draeger, S. Roeding, and T. Brixner, "Rapid-scan coherent 2D fluorescence spectroscopy," Opt. Express **25**(4), 3259–3267 (2017).
46. F. D. Fuller and J. P. Ogilvie, "Experimental implementations of two-dimensional Fourier transform electronic spectroscopy," Annu. Rev. Phys. Chem. **66**(1), 667–690 (2015).
47. J. O. Tollerud, C. R. Hall, and J. A. Davis, "Isolating quantum coherence using coherent multi-dimensional spectroscopy with spectrally shaped pulses," Opt. Express **22**(6), 6719–6733 (2014).
48. J. D. Gaynor, T. L. Courtney, M. Balasubramanian, and M. Khalil, "Fourier transform two-dimensional electronic-vibrational spectroscopy using an octave-spanning mid-IR probe," Opt. Lett. **41**(12), 2895–2898 (2016).
49. T. A. A. Oliver, N. H. C. Lewis, and G. R. Fleming, "Correlating the motion of electrons and nuclei with two-dimensional electronic-vibrational spectroscopy," Proc. Natl. Acad. Sci. U.S.A. **111**(28), 10061–10066 (2014).
50. G. Cerullo, M. Nisoli, S. Stagira, and S. De Silvestri, "Sub-8-fs pulses from an ultrabroadband optical parametric amplifier in the visible," Opt. Lett. **23**(16), 1283–1285 (1998).
51. X. Dai, M. Richter, H. Li, A. D. Bristow, C. Falvo, S. Mukamel, and S. T. Cundiff, "Two-Dimensional Double-Quantum Spectra Reveal Collective Resonances in an Atomic Vapor," Phys. Rev. Lett. **108**(19), 193201 (2012).
52. T. Suzuki, R. Singh, M. Bayer, A. Ludwig, A. D. Wieck, and S. T. Cundiff, "Coherent Control of the Exciton-Biexciton System in an InAs Self-Assembled Quantum Dot Ensemble," Phys. Rev. Lett. **117**(15), 157402 (2016).
53. G. Moody, I. A. Akimov, H. Li, R. Singh, D. R. Yakovlev, G. Karczewski, M. Wiater, T. Wojtowicz, M. Bayer, and S. T. Cundiff, "Coherent Coupling of Excitons and Trions in a Photoexcited CdTe/CdMgTe Quantum Well," Phys. Rev. Lett. **112**(9), 097401 (2014).
54. R. Augulis and D. Zigmantas, "Two-dimensional electronic spectroscopy with double modulation lock-in detection: enhancement of sensitivity and noise resistance," Opt. Express **19**(14), 13126–13133 (2011).
55. W. Xiong and M. T. Zanni, "Signal enhancement and background cancellation in collinear two-dimensional spectroscopies," Opt. Lett. **33**(12), 1371–1373 (2008).
56. T. L. Courtney, S. D. Park, R. J. Hill, B. Cho, and D. M. Jonas, "Enhanced interferometric detection in two-dimensional spectroscopy with a Sagnac interferometer," Opt. Lett. **39**(3), 513–516 (2014).
57. I. A. Heisler, R. Moca, F. V. A. Camargo, and S. R. Meech, "Two-dimensional electronic spectroscopy based on conventional optics and fast dual chopper data acquisition," Rev. Sci. Instrum. **85**(6), 063103 (2014).
58. E. Cassette, J. C. Dean, and G. D. Scholes, "Two-Dimensional Visible Spectroscopy For Studying Colloidal Semiconductor Nanocrystals," Small **12**(16), 2234–2244 (2016).
59. T. A. Gellen, J. Lem, and D. B. Turner, "Probing Homogeneous Line Broadening in CdSe Nanocrystals Using Multidimensional Electronic Spectroscopy," Nano Lett. **17**(5), 2809–2815 (2017).
60. V. I. Klimov, "Spectral and dynamical properties of multiexcitons in semiconductor nanocrystals," Annu. Rev. Phys. Chem. **58**(1), 635–673 (2007).

1. Introduction

Two-dimensional electronic spectroscopy (2DES) is a powerful tool for studying the excited-state dynamics in various material systems. By measuring the third-order nonlinear optical response as a function of the excitation and emission frequencies as well as the waiting time, 2DES provides insight about the effect of quantum coherence in the electronic dynamics [1–4]. 2DES enables direct characterization of many critical parameters that describe quantum effects in complex systems, such as homogeneous linewidths of electronic transitions [4–6], many-body correlations [7–9] in confined semiconductor nanostructures, and electronically and vibronically coherent energy/charge transfer in photosynthetic systems [10–17] and organic solar harvesters [18–20]. The valuable knowledge of quantum dynamics accessed by 2DES has stimulated rapidly-growing interest in using coherence to enhance chemical, bio-physical and optoelectronic functions [17, 21–23].

Optics EXPRESS

2DES experiments detect the weak third-order nonlinear optical response induced by three incident pulses A, B and C in an appropriate sequence with variable and phase-stable time delays [4, 5, 24]. The delay between pulses A and B is called the coherence time (τ), while the delay between pulses B and C is the population (or waiting) time (T). The third-order nonlinear polarization emits a field, which is detected in amplitude and phase by heterodyning it with a phase-locked local oscillator. It is essential to establish phase locking between pulses A and B, and between pulse C and the local oscillator. While in most designs phase stability has been accomplished using passively phase-stable approaches with a diffraction optics [25, 26], a pulse shaper [27, 28], a birefringent wedge pair [29, 30], or the phase difference evaluation from interferogram of a reference cw laser [31, 32], active phase locking method has enabled real-time evaluation of the phase variations between the pulses [33–35]. In addition, the active phase-locking approach overcomes the limit on the range of delay between A and B common in the passive approaches.

A number of schemes for 2DES have been proposed and demonstrated in a non-collinear box geometry [25, 26, 33, 36–38], a partially-collinear pump-probe geometry [27–30, 39, 40], or a full-collinear phase modulation geometry [41–45] (for a review, see Ref [46].). The box geometry is most widely used. The signals due to different quantum pathways can be well separated in time domain by the pulse sequence and/or in space by phase matching. The fully non-collinear propagation of four beams allows the independent control of the polarization of each pulse. However, the box geometry can only be implemented with pulses of a same color unless extra modulators are added to shape the spectra of individual pulses [47], limiting the range of accessible optical transitions. In contrast, the pump-probe geometry can be easily set up with different colors of the pump and probe beams. Therefore, the correlation between transitions of very different energy scale can be studied. For instance, the electronic and vibronic transitions can be investigated under resonant excitations simultaneously with the 2D electronic-vibrational spectroscopy based on a pump-probe configuration [48, 49]. Nevertheless, self-heterodyne detection with the probe beam as the local oscillator will include the pump-probe background, demanding additional efforts to isolate the 2D signal. Moreover, the collinear alignment of the two pump pulses A and B in most available setups make it challenging to set different polarizations of the two pulses.

Here we introduce a novel approach to 2DES which combines active phase locking and the broadband two-color pump-probe geometry with precise phase correction. The two pump pulses are created using a Mach-Zehnder interferometer that is phase stabilized by active feedback electronics. The separated paths in the interferometer make it possible to individually manipulate the two pump pulses. Taking advantage of this, we improve the signal-to-noise ratio by efficient suppression of scattering noise with double modulation of the two pump pulses. Moreover, a pair of quartz wedges and a compensation plate installed in the two arms of the interferometer allow to precisely manipulate the phase difference between the two pump pulses, enabling one to recover the 2DES rephasing and non-rephasing signals. By employing two non-collinear optical parametric amplifiers (NOPAs) as the pump and probe sources, we demonstrate the 2DES approach on a solution sample of CdSe/ZnS nanocrystals. Our setup combines the merits of the two geometries with robust phase stabilization, ultrafast time-resolution (< 10 fs), two-color operation, long delay scans, individual polarization manipulation and the ease of implementation.

2. Experimental implementation

The layout of our setup is shown in Fig. 1. The 2DES setup is based on the two-color pump-probe geometry with pump and probe beams from two home-built NOPAs pumped by a regenerative amplifier (Libra, Coherent Inc) which produces pulses at 800 nm with 1 kHz repetition rate [50]. The spectrum of each NOPA output can be tuned over 500-780 nm with more than 100 nm spectral coverage, which can support sub-10 fs pulses after compression by

Optics EXPRESS

chirped mirrors. The two independently tunable NOPAs enable our setup to work in either single-color or two-color modes.

2DES probes the third-order nonlinear optical response induced by a sequence of three pulses (A, B and C) with tunable time delay τ and T. We feed the output of NOPA 1 into a Mach-Zehnder interferometer to generate the pulses A and B with precisely locked relative phase and controllable delay τ. The interferometer is implemented by directly mounting optical elements on an aluminum plate for stabilization. A continuous-wave (cw) laser (472.9 nm) beam co-propagates along the path of the ultrashort pulses in the interferometer with a slight vertical shift. The interference signal from the cw laser is used as a reference monitoring the relative path lengths of the interferometer. To achieve phase locking of the two excitation pulses, we actively lock the interferometer with a feedback loop following the approach used in the JILA-MONSTR [33]. Briefly, the interference between the cw beams traveling through each arm provides an error signal that is amplified by a high-speed servo controller (LB1005, Newport) to drive the piezoelectric transducer to achieve the phase stabilization. The feedback loop is disengaged to allow the τ-stage to be moved to a position and then reengaged to record the signal at a specific τ. The scanning range of τ is only limited by the travel range of translation stage, which is of great meaning for studying the systems with long dephasing times such as atomic vapors [51] and semiconductor nanostructures at cryogenic temperature [52, 53].

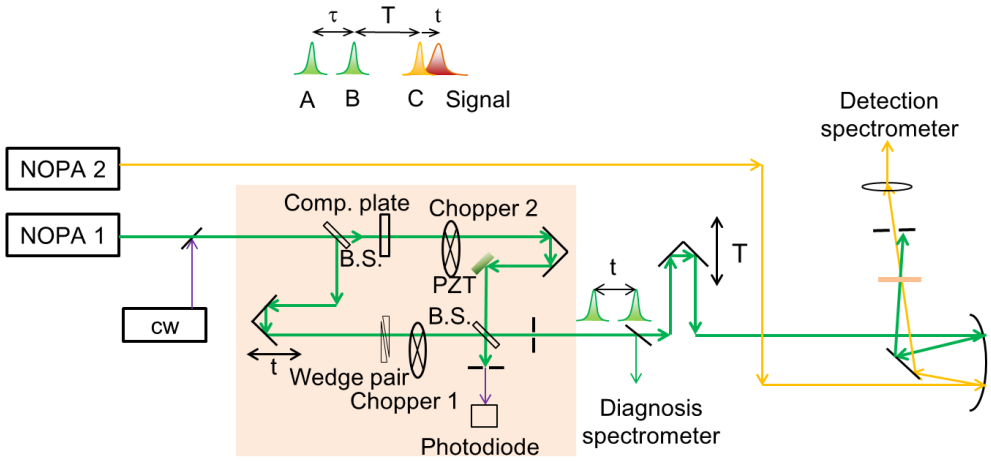

Fig. 1. Experimental setup with two independently tunable NOPAs providing pump and probe pulses. The Mach-Zehnder interferometer creates the first two excitation pulses separated by a variable delay τ. Additional delay line sets the delay T between the two pump pulses and the probe. The cw laser co-propagating along the same path of pump beam with a slight vertical shift provides diagnostic information. The insert shows the pulse sequence at the sample. A pair of quartz wedges and a compensation plate are added to the two arms for phase correction. Two choppers separately modulate the excitation pulses to suppress the scattering noise and the background of the pump-probe signal. A small portion of the two collinear excitation pulses is routed to a fiber spectrometer for real time diagnosis. The transmitted probe light is recorded by a kHz CCD. All optical elements in the interferometer are mounted directly on a same aluminum plate for mechanical stability.

The two collinear pump pulses and the probe are non-collinearly focused on the sample. The spectrum of the transmitted probe, spatially selected by an iris, is analyzed by a spectrometer equipped with a fast CCD camera (Entwicklungsburo Stresing), working at 1 kHz for acquiring the 2D spectrum on the emission axis ω_t in a pulse-to-pulse mode. After scanning τ, the 2D spectrum is generated by Fourier transformation along τ axis to obtain the excitation frequency ω_τ, where under sampling is used for the measurement in the range of

Optics EXPRESS

500-780 nm because the shortest step in τ scan is the wavelength of the cw laser. Two mechanical choppers synchronized to the laser modulate the two pump beams in the arms of the interferometer with great care taken to avoid disturbing the cw laser, which can efficiently suppress the scattering noise and the pump-probe background.

The spectral interferogram of the two pump pulses is monitored by reflecting a small portion into a fiber spectrometer, which is employed as a reference to retrieve the phase difference between the two excitation pulses. A quartz wedge pair and a compensation plate are introduced into the two arms of the interferometer to manipulate the initial phase difference between the two pump pulses as discussed in Section 3.

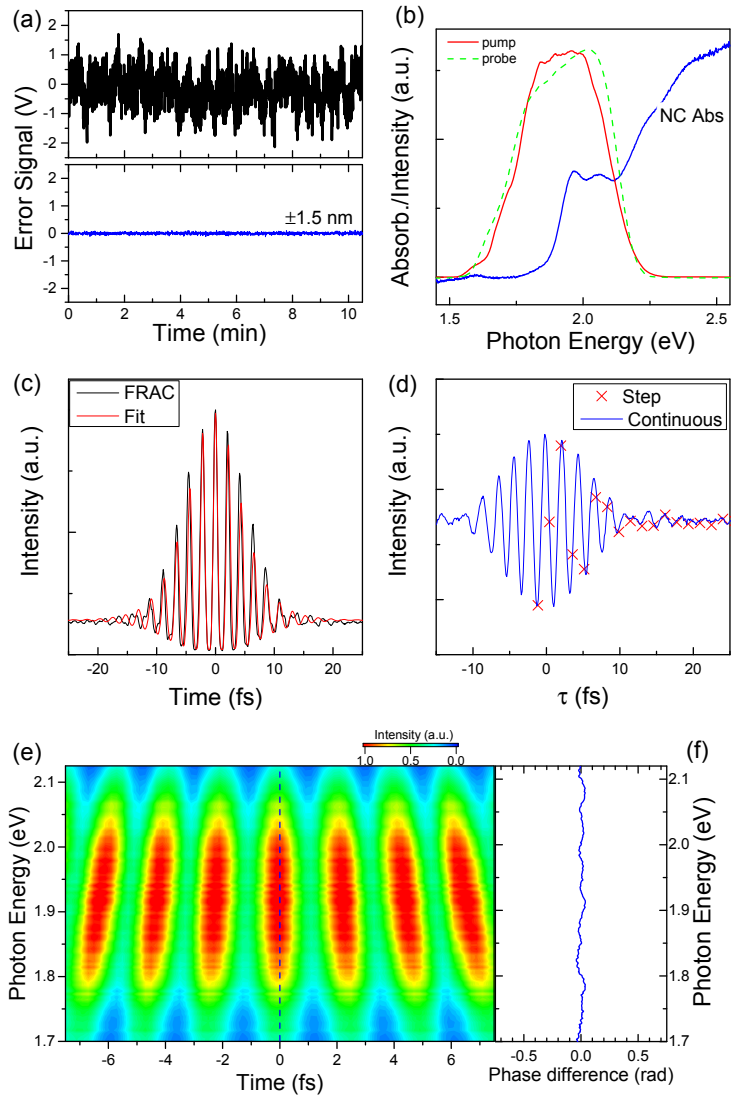

Fig. 2. (a) The error signals for the interferometer recorded for 10 minutes without (top) and with (bottom) active stabilization engaged. (b) The spectra of the pump and probe pulses and the absorption of nanocrystals for testing the setup. (c) FRAC trace of the pump pulse and a $sech^2$- fit curve show the pulse width is ~6.5 fs. (d) The diagnostic interferogram between the two pump pulses during a continuous scan (without active stabilization) or a step scan (with active stabilization). (e) The interferometer spectra of the two excitation pulses with phase correction. (f) The phase distortion is less than 0.05 rad over the broadband spectral range of the excitation pulses.

Optics EXPRESS

To test the validity of the setup, we perform experiments on a sample of core-shell CdSe/ZnS nanocrystals in toluene solution. We first tested the active stabilization of the interferometer. Figure 2(a) compares the error signals recorded with the active feedback loops disengaged and engaged. The variation in the locked error signal corresponds to phase stabilization better than λ/300 for the range of pump wavelength. The output wavelength of the pump NOPA is tuned to cover the major features of the sample absorption [Fig. 2(b)]. The pulses are compressed to near the Fourier transform limit at the sample position as characterized via fringe resolved autocorrelation (FRAC) by replacing the sample with a β-barium borate crystal. The typical retrieved temporal duration of the pulse is ~6.5 fs [Fig. 2(c)], making the temporal resolution in T-axis better than 10 fs. Figures 2(d)-2(f) show frequency-resolved and integrated spectral interferograms of the two excitation pulses. The frequency-integrated interferogram recorded as a function of τ with feedback loop engaged is compared to that recorded by a continuous scan [Fig. 2(d)], which can be adopted to precisely determine the delay and phase difference between the two pump pulses. The consistent results of interferogram recorded with and without (continuous scan) suggest that it is valid to retrieve the phase difference between two pump pulses based on the interferogram obtained by the phase-locked scan. By properly configuring the wedge pair, the phase difference between the two excitation pulses can be reset at zero τ delay over the whole spectral range with phase difference less than 0. 05 rad [Figs. 2(e) and 2(f))].

3. Results and discussion

3.1. Signal recovery and noise suppression

The noise caused by scattering of the incident pump pulses is a common issue in the 2DES. Different approaches have been introduced to recover the relatively weak signals [28, 29, 33, 54]. In a pump-probe geometry, the probe beam is also used as the local oscillator for heterodyne detection of the nonlinear optical response. The pump-probe signals produced by individual excitation pulses are also detected in this case. To reduce the unwanted pump-probe signals, the methods of polarization discrimination [27, 55] or using a Sagnac interferometer [56] have been previously applied. In our setup, the 2DES signal is in principle detectable by simultaneously modulating the two pump pulses. However, such a single modulation approach will also detect scattering noise and unwanted pump-probe signals. Exploiting the separated optical paths in the two arms of the interferometer, we can separately modulate the two pump beams. Such a double modulation is efficient in improving the signal-to-noise ratio [57]. As shown in Fig. 3(a), the choppers 1 and 2 modulate the A and B beams at 250 and 500 Hz synchronized to the laser, respectively. During a measurement cycle, four different spectra are recorded simultaneously with the synchronization signal from the choppers. During timeframe 1, the spectrum (Sig_1) includes the four-wave mixing signal, the local oscillator, the scattering of the pulses A or B and the unwanted pump-probe signals caused by the pulses A and B; During timeframe 2, the spectrum (Sig_2) includes the local oscillator, the scattering of pulse A and the unwanted pump-probe signal caused by the pulse A; During timeframe 3, the spectrum (Sig_3) includes the local oscillator, the scattering of the pulse B and the unwanted pump-probe signal caused by the pulse B; During timeframe 4, the spectrum (Sig_4) includes the local oscillator only. The interference between four-wave mixing signal and the local oscillator (i.e., the self-heterodyne detected weak nonlinear optical response) can thus be extracted as $Sig = (Sig_1 - Sig_4) - (Sig_2 - Sig_4) - (Sig_3 - Sig_4) = Sig_1 - Sig_2 - Sig_3 + Sig_4$. The obtained spectrum is transferred to the time domain by Fourier transformation and the noise is further reduced in time domain by eliminating the scattering residual. After this procedure, subtle scattering noise due to the interference between the scattered light of the two excitation pulses can be largely eliminated by subtracting a spectrum recorded with negative waiting time (i.e., T = - 2000 fs). To test this approach, we perform experiments on a nanocrystal sample with intentionally-introduced scattering centers on the cuvette surfaces. Figures 3(b) and 3(c) compare the absorptive 2DES spectra obtained

Optics EXPRESS

by the methods of single modulation and double modulation, respectively. The signal-to-noise ratio is dramatically improved by double modulation with the signal distortion and diagonal streaks well suppressed. The approach can be naturally extended to two-color measurement. Figures 3(d) and 3(e) show the different spectra of pump and probe beams, respectively. 2D spectrum of CdSe/ZnS NCs recorded in the two-color mode exhibits negative signals due to the excited-state absorption.

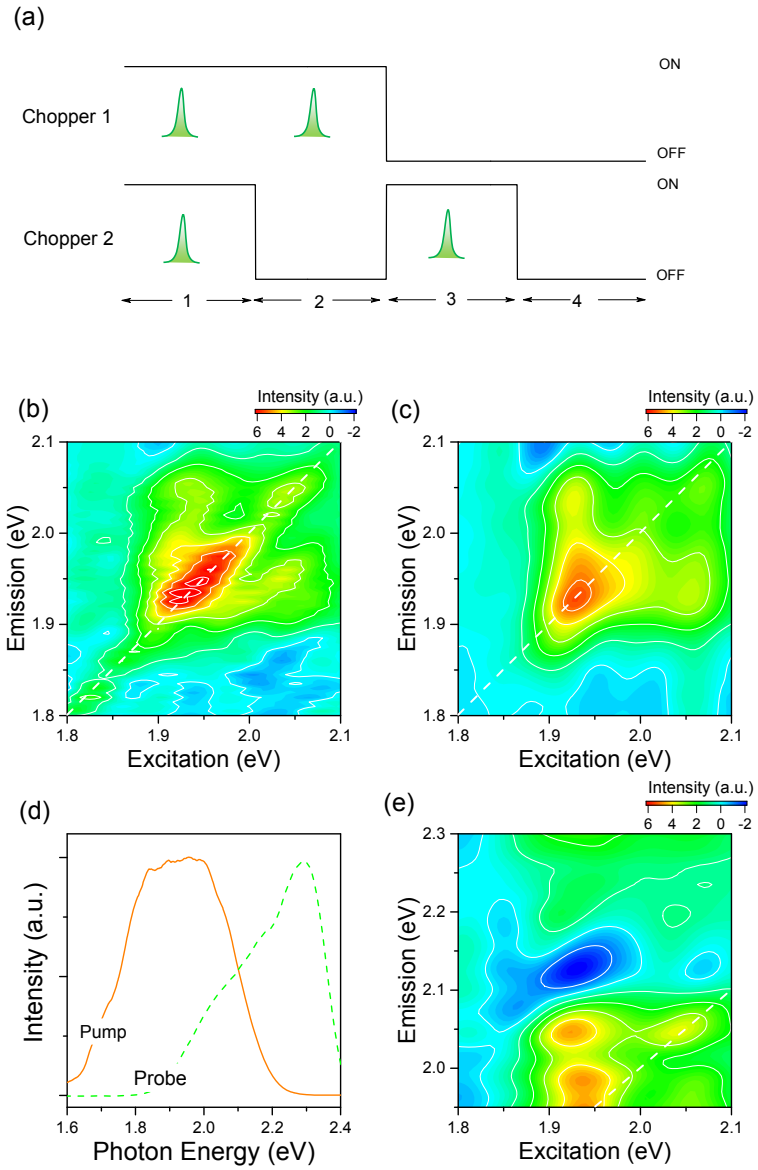

Fig. 3. (a) The sequence of two excitation pulses modulated by two choppers. Absorptive 2D spectra of a nanocrystal sample with intentionally introduced scattering centers acquired by the methods of single modulation (b) and double modulation (c). All the data are captured at a waiting time T = 60 fs. The 2D spectra as a function of T are available in a movie (see Visualization 1). (d) Spectra of pump and probe beams for two-color 2D spectroscopy. (e) Absorptive 2D spectrum of the CdSe/ZnS NC sample.

Optics EXPRESS

The obtained 2D spectra of CdSe/ZnS NCs are consistent with literature results characterized by established approaches [58, 59]. The two diagonal peaks correspond to the two excitonic transitions (i.e., $1S_{1/2}(e)$ - $1S_{3/2}(h)$ and $1S_{1/2}(e)$ - $2S_{3/2}(h)$) sharing a common excited level in the conduction band [60]. The coherent coupling between the two excitonic transitions is manifested as the off-diagonal features [Fig. 2(c)]. The 2D spectra are recorded as a function of waiting time (T) (see Visualization 1). The signals exhibit oscillations along T due to strong vibrational couplings [58, 59].

3.2. Phase correction

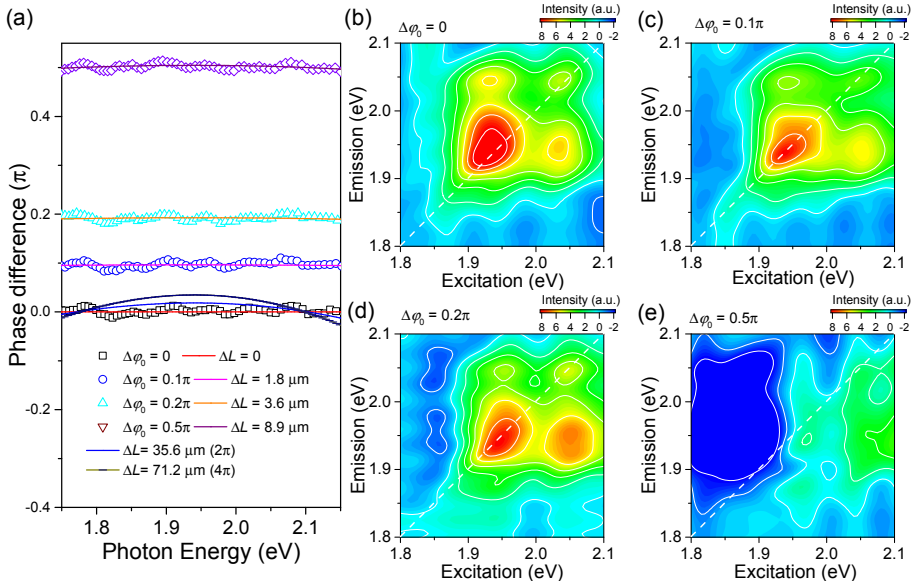

Fig. 4. Phase correction. (a) Photon-energy dependent phase errors between two excitation pulses compared with the results calculated with different thickness of quartz. Multiples of 2π in phase difference are removed in the plot. The error in phase estimation is better than 0.05 rad. (b)-(e) 2D spectra generated with different values of phase errors.

Phase retrieval is indispensable for 2DES. In the pump-probe geometry, the two excitation pulses are interchangeable with the same wave-vector. The 2DES spectra can thus be fully obtained by scanning positive τ values. The four-wave mixing signal co-propagates with the probe beam. The spectral phase difference between the two pump pulses, $\Delta\varphi_{BA}(\omega_\tau)$, is required for phase correction of 2DES spectra. In principle, the two excitation pulse replicas at zero τ delay have a flat spectral dependence of zero phase difference over the whole wavelength range [Fig. 2(f)]. When the feedback loop is engaged, the $\tau = 0$ sampling point is not included in the discrete scanning sampling points, resulting a phase difference $\Delta\varphi_{BA}(\omega_\tau) = \omega_\tau\tau_0$ where τ_0 is the delay at the scanning point closest to zero. We acquire interferograms of the two pump pulses by the diagnostic spectrometer for continuous and step scanning modes. The value of τ_0 can be evaluated by finding the point with the flattest phase in the spectral domain. The phase corrected 2DES spectrum is,

$$S(\omega_\tau, T, \omega_t) = S_{Raw}(\omega_\tau, T, \omega_t)\exp\left[-i\Delta\varphi_{BA}(\omega_\tau)\right], \quad (1)$$

where $S_{Raw}(\omega_\tau, T, \omega_t)$ is the as-measured spectrum. During the acquisition of the 2DES signal at each selected T delay, we record the interferograms of the pump pulse pair at the same time via a diagnostic spectrometer to reduce possible effects caused by long-time

Optics EXPRESS

instability. The spectral phase difference $\Delta\varphi_{BA}(\omega_\tau)$ can be updated from this data and then be used to perform phase retrieval of the 2D spectrum at each given T delay in real time.

In the above discussion, it is assumed that τ_0 is the only factor causing the initial phase difference between A and B pulses. At zero τ delay, the spectrally-resolved interferogram of the two pump pulses exhibits a zero phase difference over the broad spectral range [Figs. 2(e) and 2(f)]. However, it is generally more complicated since a tiny difference between the optical paths of two arms in the interferometer may cause additional phase distortion. As a consequence, the flat phase in spectral domain may appear with non-zero value. In-depth analysis suggests that such phase difference is probably caused by a slight thickness difference between the quartz substrates of the two beam splitters in the interferometer or a tiny error in the beam alignment. With a small thickness difference ΔL of quartz in the two arms, the spectral phase difference should be rewritten as,

$$\Delta\varphi_{BA}(\omega_\tau, \Delta L) = \omega_\tau(\tau_0 - n(\omega_\tau)\Delta L / c). \tag{2}$$

The thickness difference causes an optical delay in τ which can be corrected following Eq. (1). However, the dispersion of the refractive index induces additional phase distortion that cannot be described by a single parameter τ_0. Here, we consider the dispersion of the refractive index ($n(\omega)$) near the center frequency ω_0, i.e.,

$$n(\omega) = n(\omega_0) + (\omega - \omega_0)\frac{\partial n}{\partial \omega} + \cdots. \tag{3}$$

The spectral phase difference can be rewritten,

$$\begin{aligned}\Delta\varphi_{BA}(\omega_\tau, \Delta L) &= \omega_\tau(\tau_0 - n(\omega_0)\Delta L / c - \frac{\partial n}{\partial \omega}\omega_0 \Delta L / c) - \frac{\partial n}{\partial \omega}(\omega_\tau - \omega_0)^2 \Delta L / c + \frac{\partial n}{\partial \omega}\omega_0^2 \Delta L / c, \\ &\approx \omega_\tau \tau_0' + \Delta\varphi_0\end{aligned} \tag{4}$$

where

$$\tau_0' = \tau_0 - n(\omega_0)\Delta L / c - \frac{\partial n}{\partial \omega}\omega_0 \Delta L / c, \tag{5}$$

and

$$\Delta\varphi_0 = \frac{\partial n}{\partial \omega}\omega_0^2 \Delta L / c. \tag{6}$$

It is a good approximation for small ΔL since $(\omega_\tau - \omega_0)^2/\omega_0^2 < 0.01$ in the spectral range of the excitation pulses. To avoid this side effect, we place a wedge pair in one arm and a compensation plate in the other to manipulate the phase difference between the two excitation pulses. By adjusting the wedge thickness, the phase difference can be finely tuned as shown in Fig. 4(a). Phase manipulation over a full cycle (i.e., $-\pi \le \Delta\varphi_0 \le \pi$) requires less than 20 μm additional thickness of quartz. The effect of its group delay dispersion on pulse duration is negligible. The spectral dispersion can be very well reproduced by Eq. (2) with different thicknesses of quartz. Such phase correction is critical to generate properly phased 2DES spectra. Figures 4(b)-4(e) compare the absorptive 2DES spectra obtained with different phase differences. The phase distortion ($\Delta\varphi_0$), if not corrected, may significantly distort the absorptive 2DES spectra as it mixes the dispersive parts of rephasing and non-rephasing signal as discussed in the following section.

Optics EXPRESS

3.3 Rephasing and non-rephasing signal recovery

In the pump-probe geometry, the collinear configuration makes the A and B pump pulses indistinguishable. It is easy to generate the absorptive 2DES spectrum since it inherently measures the sum of rephasing and non-rephasing spectra. However, with the additional distorted phase, the detected signal is,

$$S^{\Delta\varphi_0}(\tau,T,t) \propto S_{\mathrm{R}}(\tau,T,t)e^{-i\Delta\varphi_0} + S_{\mathrm{NR}}(\tau,T,t)e^{i\Delta\varphi_0}. \quad (7)$$

The additional phase distortion causes phase roll in the 2D signal. The 2D spectrum $\mathrm{S}^{\Delta\varphi_0}(\omega_\tau,T,\omega_t)$ obtained by direct Fourier transform of $\mathrm{S}^{\Delta\varphi_0}(\tau,T,\omega_t)$ is no longer purely absorptive signal but mixed with real and imaginary part of the rephasing ($S_R(\tau,T,t)$) and non-rephasing ($S_{NR}(\tau,T,t)$) parts, leading to a strong dependence of the 2D map on the distorted phase [Fig. 4].

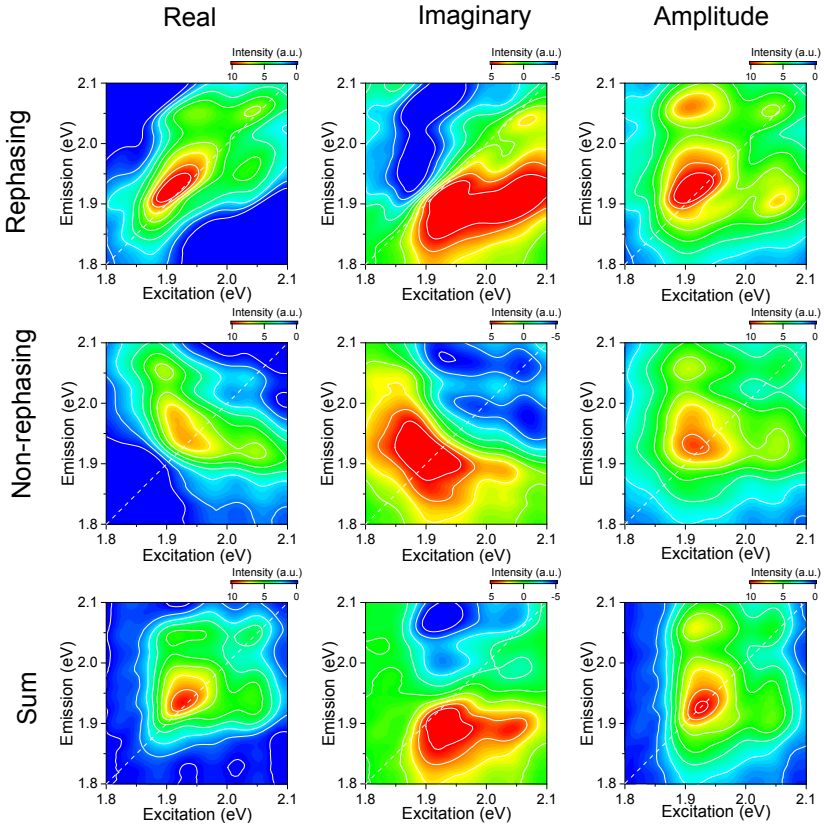

Fig. 5. Separation of the rephasing and non-rephasing signals from experimental data recorded with $\Delta\varphi_0 = 0$ and $\pi/2$.

We find the phase roll can be employed to separate the rephasing and non-rephasing contributions in the measurement. Rephasing and non-rephasing signals connect directly to Feynman diagrams of specific quantum pathways, which are of particular interest for understanding the physics underlying the experimental data. Nevertheless, it is challenging to separate them in the pump-probe configuration since A and B pulses are interchangeable in the measurement. It has been proposed to separate the rephasing and non-rephasing spectra by combining the signals recorded with phase differences of 0 and $\pi/2$ [27, 41], i.e.,

Optics EXPRESS

$$S_{\mathrm{R}}(\omega_\tau,T,\omega_t) \propto S^{0}(\omega_\tau,T,\omega_t)+iS^{\pi/2}(\omega_\tau,T,\omega_t), \tag{8}$$

$$S_{\mathrm{NR}}(\omega_\tau,T,\omega_t) \propto S^{0}(\omega_\tau,T,\omega_t)-iS^{\pi/2}(\omega_\tau,T,\omega_t). \tag{9}$$

Previously, such operation in pump-probe based 2D setup has been done by Ogilvie et al. with a pulse shaper [27]. In our setup, we find such phase manipulation can be also done by simply adjusting the wedge pair. Briefly, $\Delta\varphi_0 = 0$ can be obtained by setting $\Delta L = 0$, while $\Delta\varphi_0 = \pi/2$ can be approached by setting $\Delta L = 8.9$ μm respectively. The raw data $S^{0}_{Raw}(\tau,T,\omega_t)$ and $S^{\pi/2}_{Raw}(\tau,T,\omega_t)$ are transferred into the time domain as $S^{0}(\tau,T,t)$ and $S^{\pi/2}(\tau,T,t)$ to ensure causality. In order to avoid the potential errors caused by the uncertainty of τ, we transform the time domain results with phase correction into the frequency domain spectra $S^{0}(\omega_\tau,T,\omega_t)$ and $S^{\pi/2}(\omega_\tau,T,\omega_t)$, and perform the linear combination to extract the rephasing and non-rephasing signals. Figure 5 shows an example demonstrating the successful separation of the rephasing and non-rephasing contributions from the raw data recorded with $\Delta\varphi_0 = 0$ and $\Delta\varphi_0 = \pi/2$. In principle, the precise modulation of $\Delta\varphi_0$ can be potentially employed to do phase cycling to suppress the scattering noise [33].

4. Conclusion

In summary, we have demonstrated a novel configuration for broadband 2DES based on a partially collinear pump-probe geometry with pump pulse replicas generated from an actively-stabilized Mach-Zehnder interferometer. The setup integrates major advantages of the available non-collinear box and partially-collinear pump-probe geometries. The design is not only easy for optical alignment in the pump-probe geometry but also convenient for individually manipulating the amplitude, phase, polarization and other degrees of freedom of the two pump beams. The separated optical paths of two pump beams in the interferometer prove to be instrumental for noise suppression and phase control. The pulse-to-pulse data acquisition is more time efficient, taking less than one minute for each 2D spectrum. The approach can be naturally extended to the shorter or longer wavelength range with proper optical coatings. Similar to the box geometry, the rephasing and non-rephasing 2D signals can be easily extracted in our setup. In the future, recording of the double-quantum signal may be possible if the phase locking between pump and probe beam is established.

Funding

National Key R&D Program of China Grant No. 2017YFA0303700 and 2013CB932903; National Natural Science Foundation of China through Grant No. 11574140, 11227406, 91233103, 11621091, and 11474178; Jiangsu Provincial Funds for Distinguished Young Scientists through Grant N. BK20160019; Horizon 2020 (654148, Laserlab-Europe).

Acknowledgments

CZ acknowledges Dr. Hebin Li, and Dr. Tobias Brixner for sharing technical details and Dr. Xuewei Wu for his technical assistance.